Available online at www.sciencedirect.com

ScienceDirect

IFAC PapersOnline CONFERENCE PAPER ARCHIVE

IFAC PapersOnLine 55-38 (2022) 113–119

An Experimental Study on MPC based Joint Torque Control for Flexible Joint Robots

Christian Ott * **Fabian Beck** ** **Manuel Keppler** **

* *Automation & Control Institute, TU Wien, Vienna, Austria, (email: christian.ott@tuwien.ac.at)*

** *Institute of Robotics and Mechatronics, German Aerospace Center (DLR), Wessling, Germany, (email: fabian.beck@dlr.de, manuel.keppler@dlr.de)*

Abstract: This paper presents an experimental evaluation of joint torque control in a flexible joint robot using a model predictive control approach. The control of elastic robots is challenging due to the underactuated nature of the connected link and motor dynamics. A typical solution is to formulate the controller in a cascaded way with an outer loop controller for the nonlinear link side dynamics in combination with an inner loop controller for the joint torque. In this paper the inner loop torque controller utilizes a model predictive control design in order to take actuator constraints into account and, in case of a special choice of the torque reference and control gains, to avoid the computation of higher time derivatives in the desired joint torque. We compare two different controller implementations, which differ in the choice of the reference model. In particular, we investigate on the use of the natural open loop dynamics for the reference model. The controllers are evaluated in detail using a simulation study as well as in experiments on a single joint testbed.

Keywords: Model Predictive Control, Flexible Joint Robots, Torque Control

1. INTRODUCTION

The control of robots with joint elasticity is a classical topic in robot control. Elastic robots are a specific class of underactuated mechanical systems, which consist of a nonlinear rigid-body dynamics in connection with the elastic actuator dynamics. While joint elasticity was originally considered as a disturbance to the rigid-body robot model, novel mechatronic actuator designs, like variable impedance actuators, deliberately incorporate elastic components in the robot drive train (Vanderborght et al. (2013)). This is often motivated by the improved physical robustness of an elastic actuator against external impacts, or by the potential to utilize the energy storage capability in elastic actuators for realizing energetically efficient (periodic) motions (Liu et al. (2020)).

Early control approaches for elastic robots include controllers developed based on approximative models such as in the singular perturbation approach (Siciliano and Book (1988)) or controllers that apply a complete or partial dynamic inversion (De Luca (1988); Palli et al. (2008)). Amongst these approaches, cascaded controller designs, e.g. based on feedback linearization or backstepping techniques, showed strong theoretical stability properties, but were practically effected by the need for link acceleration and jerk in the implementation of the control law (Ott et al. (2003)). Passivity based techniques were originally restricted to purely motor based feedback (Tomei (1991)), and later extended by proportional and derivative feedback actions on the measured joint torque (Ott et al. (2008)). These approaches were especially well suited for robots with explicit joint torque sensors. More recently, the Elastic Structure Preserving (ESP) control framework was proposed with the aim to preserve the natural actuation compliance, while realizing a closed loop behavior that incorporates some desired control actions such as link side damping and task space stiffness (Keppler et al. (2018, 2022)). The original ESP control approach followed a similar line of reasoning as the controllers from De Luca and Flacco (2010, 2011) which were developed based on the physical equivalence principle. The strength of these control approaches clearly lies in their experimentally proven robustness against modeling uncertainties (Keppler et al. (2018)), which can be explained by the preservation of the (undamped) open loop compliance in the (well damped) closed loop dynamics.

One of the drawbacks of the above-mentioned approaches is the requirement of computing the first and second time derivative of the desired torque, which act as feed-forward control actions in the torque controller. This is feasible for simple joint-level controllers like joint impedance controllers, assuming that an estimation of joint acceleration and jerk can be computed from the available measurements (e.g. motor and link side position as well as joint torque) in a model-based way. However, if the desired torque is computed from a more complex control approach,

⋆ This project has received funding from the European Research Council (ERC) under the European Union's Horizon 2020 research and innovation programme (grant agreement No. 819358). The first and second author contributed equally.

10.1016/j.ifacol.2023.01.142

such as an optimization based whole-body control algorithm for multiple (maybe even hierarchic) tasks (Sentis et al. (2010); Henze et al. (2016)), the analytic computation of these time derivatives often is not possible. Simply neglecting these feed-forward torques implicitly results in a singular perturbation approach and would require a separation of the bandwidth of the desired rigid-body behavior and the underlying joint torque controller.

The main motivation for the presented work is to test a model predictive control (MPC) formulation for the inner loop torque controller, which utilizes a prediction of the system dynamics over some time horizon instead of using the instantaneous higher derivatives of the desired torques. The second and higher time derivatives are completely avoided in the proposed MPC scheme, while the first time derivative might be used depending on the reference design and gain selection. MPC formulations have been successfully employed in various industrial contexts, see for example Qin and Badgwell (2003). Using a prediction of a cost function is not new in the control of flexible joint robots and was already studied by Kuntze et al. (1986). Compared to existing approaches, such as Ghahramani and Towhidkhah (2009), the proposed approach formulates the MPC problem only for the linear torque dynamics in combination with a compensation of the link-side coupling and motor-side friction instead of controlling the link and motor dynamics in a combined manner.

In contrast to the state-of-the-art approaches for cascaded control of elastic robots, the MPC-based formulation also allows to incorporate limitations on the control input (motor torque) and other state constraints in the design. Since the desired torque is assumed to be available only for the current time instant and not for the whole prediction horizon, the question arises how to choose the reference model in the MPC formulation. To this end we compare two different reference models, namely a simple constant reference with a dynamic reference which follows the natural open loop torque dynamics. The main contributions of the paper are

- an MPC-based formulation of a joint torque controller that allows for including constraints on the control-input and state, as well as
- the comparison of different reference models in simulation and experiments.

The paper is organized as follows. Section 2 presents the problem formulation and the model. The MPC based controller formulation is presented in Section 3. Simulation and experimental results are reported in Section 4 and 5. Finally, Section 6 summarizes the observations and concludes the paper.

2. PROBLEM FORMULATION AND MODEL DEFINITION

In this paper we consider the reduced flexible joint robot model for a series chain manipulator with n joints as proposed by Spong (1987), i.e.

$$\boldsymbol{M}(\boldsymbol{q})\ddot{\boldsymbol{q}} + \boldsymbol{C}(\boldsymbol{q},\dot{\boldsymbol{q}})\dot{\boldsymbol{q}} + \boldsymbol{g}(\boldsymbol{q}) = \boldsymbol{K}(\boldsymbol{\theta}-\boldsymbol{q}), \tag{1}$$

$$\boldsymbol{B}\ddot{\boldsymbol{\theta}} + \boldsymbol{K}(\boldsymbol{\theta}-\boldsymbol{q}) = \boldsymbol{\tau}_m + \boldsymbol{\tau}_f. \tag{2}$$

Here, $\boldsymbol{\theta} \in \mathbb{R}^n$ and $\boldsymbol{q} \in \mathbb{R}^n$ are the motor and joint angles. The rigid-body part (1) of the model contains the symmetric and positive definite inertia matrix $\boldsymbol{M}(\boldsymbol{q})$, the gravity torques $\boldsymbol{g}(\boldsymbol{q})$ and the Coriolis/centrifugal matrix $\boldsymbol{C}(\boldsymbol{q},\dot{\boldsymbol{q}})$. The joint elasticity is defined via the diagonal and positive definite stiffness matrix $\boldsymbol{K} \in \mathbb{R}^{n\times n}$. The motor dynamics contains the diagonal and positive definite motor inertia matrix $\boldsymbol{B} \in \mathbb{R}^{n\times n}$ and the motor torques $\boldsymbol{\tau}_m \in \mathbb{R}^n$, which are considered as the control input. Each motor has an upper and a lower torque limit, i.e., $\tau_{m,\min,i} < \tau_{m,i} < \tau_{m,\max,i}$, where i denotes the joint index. Furthermore, $\boldsymbol{\tau}_f$ models friction and other disturbances on the motor side, such as the viscous friction introduced by the gear.

In the model (1)-(2), the motor and link dynamics are coupled via the joint torques $\boldsymbol{\tau} = \boldsymbol{K}(\boldsymbol{\theta}-\boldsymbol{q})$ and the torque dynamics can be obtained as

$$\boldsymbol{B}\boldsymbol{K}^{-1}\ddot{\boldsymbol{\tau}} + \boldsymbol{\tau} = \boldsymbol{\tau}_m - \boldsymbol{B}\ddot{\boldsymbol{q}} + \boldsymbol{\tau}_f\ . \tag{3}$$

For the rest of the paper we assume that a desired control law for the link side dynamics is known, which generates a desired torque $\boldsymbol{\tau}_d = \boldsymbol{\tau}_d(\boldsymbol{q},\dot{\boldsymbol{q}})$. This desired torque could be achieved, e.g., by a joint torque controller based on partial feedback linearization, i.e.

$$\boldsymbol{\tau}_m = \boldsymbol{\tau} + \boldsymbol{B}\ddot{\boldsymbol{q}} - \hat{\boldsymbol{\tau}}_f + \boldsymbol{B}\boldsymbol{K}^{-1}(\ddot{\boldsymbol{\tau}}_d - \boldsymbol{K}_\tau\boldsymbol{e} - \boldsymbol{D}_\tau\dot{\boldsymbol{e}}), \tag{4}$$

with the torque error $\boldsymbol{e} = \boldsymbol{\tau} - \boldsymbol{\tau}_d$ and positive definite controller gain matrices $\boldsymbol{D}_\tau$ and $\boldsymbol{K}_\tau$. To ensure a good torque tracking performance, friction compensation is realized by a model-based disturbance observer (Kim et al. (2019)), which estimates friction and other disturbances on the motor side in form of $\hat{\boldsymbol{\tau}}_f$. The controller (4) is a theoretically appealing approach yielding the linear torque error dynamics $\ddot{\boldsymbol{e}} + \boldsymbol{D}_\tau\dot{\boldsymbol{e}} + \boldsymbol{K}_\tau\boldsymbol{e} = \boldsymbol{0}$. However, (4) can only be implemented when the first and second time derivative of $\boldsymbol{\tau}_d$ are available. This is often not the case, when the rigid-body controller is, e.g., computed by a complex whole-body control algorithm (Sentis et al. (2010)) or computed numerically via an optimization based control approach (e.g. Ramuzat et al. (2022)).

The control problem analyzed in this paper is formulated as follows: Given at each time instant a desired control torque $\boldsymbol{\tau}_d$, which is only available in its numeric form, design a joint torque controller for the model (3) which does not require the time derivatives of the desired torque and which is able to consider constraints on the control input.

3. MPC BASED JOINT TORQUE CONTROL

In this section an MPC scheme for the torque dynamics (3) is derived, which takes account of the requirements mentioned in the above defined control problem. An overview of the control architecture is displayed in Fig. 1.

3.1 QP Formulation

The torque dynamics in (3) represents a linear second order dynamics with a disturbance term $\boldsymbol{a}_q = -\boldsymbol{B}\ddot{\boldsymbol{q}} + \boldsymbol{\tau}_f$, which represents the coupling with the multi-body dynamics and friction effects. We use a pre-compensation of this disturbance

$$\boldsymbol{\tau}_m = \boldsymbol{u} + \boldsymbol{B}\ddot{\boldsymbol{q}} - \hat{\boldsymbol{\tau}}_f = \boldsymbol{u} - \hat{\boldsymbol{a}}_q \tag{5}$$

and control the remaining linear torque dynamics for each joint separately with a model predictive control approach

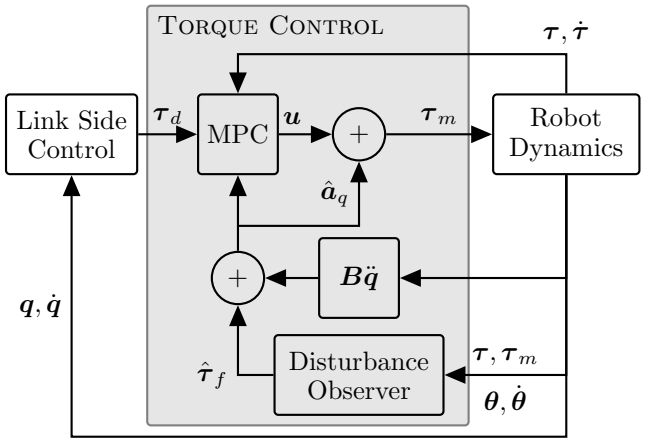

Fig. 1. Model predictive torque control architecture.

that computes the intermediate control input $\boldsymbol{u} \in \mathbb{R}^n$. Without loss of generality, we formulate the controller for the single joint case such that $\tau \in \mathbb{R}$ and $u \in \mathbb{R}$. For the formulation of the MPC problem we utilize a discrete time formulation with sampling time T and use the index k to denote the discrete time step.

The prediction model is then obtained directly from (3) and (5) as

$$\boldsymbol{x}_{k+1} = \boldsymbol{A}_d \boldsymbol{x}_k + \boldsymbol{B}_d u_k, \tag{6}$$

where the state $\boldsymbol{x}_k = [\tau_k, \dot{\tau}_k]$ contains the joint torque and its time derivative and the system matrices are given by

$$\boldsymbol{A}_d = \boldsymbol{e}^{\boldsymbol{A}_c T}, \qquad \boldsymbol{A}_c = \begin{bmatrix} 0 & 1 \\ -KB^{-1} & 0 \end{bmatrix}, \tag{7}$$

$$\boldsymbol{B}_d = \int_0^T \boldsymbol{e}^{\boldsymbol{A}_c \nu} d\nu \boldsymbol{B}_c, \qquad \boldsymbol{B}_c = \begin{bmatrix} 0 \\ KB^{-1} \end{bmatrix}. \tag{8}$$

At time step k the system state is predicted over a time horizon of N sampling intervals based on the current state $\boldsymbol{x}_k$ and the future control inputs u_{k+j} for $j = 0, \cdots, N-1$ via $\boldsymbol{x}_{k+j} = \boldsymbol{A}_d^j \boldsymbol{x}_k + \sum_{i=0}^{j-1} \boldsymbol{A}_d^{j-1-i} \boldsymbol{B}_d u_{k+i}$ which can be written in compact vectorized form as

$$\boldsymbol{X} = \boldsymbol{F}_x \boldsymbol{x}_k + \boldsymbol{F}_u \boldsymbol{U}\ , \tag{9}$$

where

$$\boldsymbol{F}_x = \begin{bmatrix} \boldsymbol{A}_d \\ \vdots \\ \boldsymbol{A}_d^N \end{bmatrix}, \quad \boldsymbol{F}_u = \begin{bmatrix} \boldsymbol{A}_d^0 \boldsymbol{B}_d & \cdots & \boldsymbol{0} \\ \vdots & \ddots & \vdots \\ \boldsymbol{A}_d^{N-1} \boldsymbol{B}_d & \cdots & \boldsymbol{A}_d^0 \boldsymbol{B}_d \end{bmatrix}, \tag{10}$$

and

$$\boldsymbol{X} = \begin{bmatrix} \boldsymbol{x}_{k+1} \\ \vdots \\ \boldsymbol{x}_{k+N} \end{bmatrix}, \qquad \boldsymbol{U} = \begin{bmatrix} u_k \\ \vdots \\ u_{k+N-1} \end{bmatrix}. \tag{11}$$

Given a reference signal for the state $\boldsymbol{r}_k \in \mathbb{R}^2$ over the prediction horizon $k = 1 \cdots N$, the model predictive controller is defined using the following optimization problem

$$\min_{u_k} \sum_{k=1}^{N} (\boldsymbol{x}_k - \boldsymbol{r}_k)^\top \boldsymbol{Q} (\boldsymbol{x}_k - \boldsymbol{r}_k) + u_{k-1}^\top R u_{k-1}, \tag{12}$$

where $\boldsymbol{Q} = \mathrm{diag}(Q_\tau, Q_{\dot{\tau}})$ and $R \in \mathbb{R}_{>0}$ are positive optimization weights. The optimization (12) is to be performed subject to the constraints [1]

$$u_{\min} < u_k < u_{\max}, \tag{13}$$

$$\boldsymbol{x}_{\min} < \boldsymbol{x}_k < \boldsymbol{x}_{\max}, \tag{14}$$

for $k = 0, \ldots, N-1$. The bounds of the virtual control input u_k are set based on the motor torque limits under consideration of the pre-compensation (5), i.e. $u_{\max} = \tau_{m,\max} - \hat{a}_q$ and $u_{\min} = \tau_{m,\min} - \hat{a}_q$.

For realtime implementation of the MPC algorithm it is important to keep the number of optimization variables small. In order to decouple the length of the prediction horizon from the number of optimization variables, one can use a different sampling time T_c for the control input than for the prediction. By choosing T and T_c in the form $T_c = MT$, where $M \in \mathbb{N}_{>0}$ this can be written as

$$\boldsymbol{U} = \boldsymbol{P}\bar{\boldsymbol{U}}, \quad \boldsymbol{P} = \begin{bmatrix} \boldsymbol{l} & \boldsymbol{0} & \boldsymbol{0} & \cdots \\ \boldsymbol{0} & \boldsymbol{l} & \boldsymbol{0} & \cdots \\ \vdots & \ddots & \ddots & \boldsymbol{0} \\ \boldsymbol{0} & \cdots & \boldsymbol{0} & \boldsymbol{l} \end{bmatrix}, \quad \bar{\boldsymbol{U}} = \begin{bmatrix} \bar{u}_k \\ \vdots \\ \bar{u}_{k+M-1} \end{bmatrix}, \tag{15}$$

with $\boldsymbol{l} = [1, 1, \cdots, 1]^T \in \mathbb{R}^M$ as a vector of length M with all elements set to 1.

In the absence of state constraints the optimization can be formulated in a compact way by the following quadratic problem (QP)

$$\min_{\bar{\boldsymbol{U}}} \bar{\boldsymbol{U}}^\top \boldsymbol{H} \bar{\boldsymbol{U}} + \boldsymbol{G}^T \bar{\boldsymbol{U}} \tag{16}$$

with the constraints

$$u_{\min} < \bar{u}_k < u_{\max}, \tag{17}$$

for $k = 0, \ldots, N-1$ and where

$$\boldsymbol{H} = \boldsymbol{P}^T (R\boldsymbol{I} + \boldsymbol{F}_u^T \bar{\boldsymbol{Q}} \boldsymbol{F}_u) \boldsymbol{P}, \tag{18}$$

$$\boldsymbol{G} = 2\boldsymbol{P}^T \boldsymbol{F}_u^T \bar{\boldsymbol{Q}} (\boldsymbol{F}_x \boldsymbol{x}_k - \boldsymbol{R}), \tag{19}$$

with $\bar{\boldsymbol{Q}} = \mathrm{d}iag(\boldsymbol{Q}, \cdots, \boldsymbol{Q}) \in \mathbb{R}^{2N \times 2N}$ and the predicted reference included in the vector $\boldsymbol{R} = (\boldsymbol{r}_{k+1}, \cdots, \boldsymbol{r}_{k+N}) \in \mathbb{R}^{2N}$.

3.2 Choice of the Reference Model

One of the key challenges in the control problem as formulated in Section 2 is the requirement to avoid any time derivatives for the desired torque τ_d. In the MPC approach this is addressed by considering the control problem over a finite time horizon. As a consequence, for exact torque tracking the desired torque should be available over the complete control horizon. This would be possible if the outer loop controller also uses a prediction over the same control horizon such as in (Meduri et al. (2022)). However, state-of-the-art whole-body controllers usually are formulated using projections or optimizations at the current time step only. In this case, an additional reference model is needed in order to generate a desired torque reference from the current command over the whole prediction horizon. Notice that the role of the reference model for tracking tasks has already been addressed in the general MPC control literature such as, e.g., in (Goodwin et al. (2011)).

[1] The vectorized inequality constraints in (14) are to be understood element wise.

A simple solution for this would be to choose a constant reference over the whole horizon, i.e. $\boldsymbol{r}_{k+j} = (\tau_{d,k}, \dot{\tau}_{d,k})$ for $j = 1, \ldots, N$. In the following we will denote this version of the controller as MCR (MPC with constant reference). Notice that while the first time derivative of the desired torque is still required for the general case, the controller formulation can be made independently of $\dot{\tau}_{d,k}$ by setting the weight $Q_{\dot{\tau}}$ to zero.

As an alternative solution, we analyze in this paper the case when the open loop behavior of the torque dynamics is utilized as a reference model. This choice is motivated by the consideration that a reference that respects the natural open loop dynamics can be simply followed without additional control action. In this way, the MPC controller should produce a "minimal" control action for reference trajectories that take the natural system dynamics into account. Based on (9), this idea can be realized via

$$\boldsymbol{R} = \begin{pmatrix} \boldsymbol{r}_{k+1} \\ \vdots \\ \boldsymbol{r}_{k+N} \end{pmatrix} = \boldsymbol{F}_x \begin{pmatrix} \tau_{d,k} \\ \dot{\tau}_{d,k} \end{pmatrix}. \tag{20}$$

However, in this case the use of the first time derivative of the desired torque is required and cannot be avoided. For the comparison in Section 4 and 5 we will denote this version of the controller as MNR (MPC with natural reference).

4. SIMULATION STUDY

In this section, the MPC with natural reference (MNR) and MPC with constant reference (MCR) are evaluated in a numerical simulation of a single joint and compared to the torque controller (4) based on partial feedback linearization (FBL). A key aspect of this study is the consideration of motor torque limitations. The dynamics of the simulated joint is given by (1) and (2), with $m = 2\,\mathrm{kgm}^2$, $B = 1.6\,\mathrm{kgm}^2$, $K = 600\,\mathrm{Nm/rad}$, and no Coriolis and gravity terms. The control input τ_m is limited to a maximal motor torque of $\pm 200\,\mathrm{Nm}$. In order to validate the control performance a simple joint compliance controller, given by

$$\tau_d = -K_d(q - q_d) - D_d\dot{q}, \tag{21}$$

is implemented, where q_d denotes the desired joint position reference. The control frequency of the link side compliance and the torque controller is 1 kHz. For both MPC schemes a prediction sampling time of $T = 5 \times 10^{-3}\,\mathrm{s}$ and a prediction horizon of $N = 10$ samples is used. The control horizon is set equal to the prediction horizon to $M = N = 10$, i.e., $\boldsymbol{P} = \boldsymbol{I}$. The stiffness of the compliance controller was selected to be $K_d = 200\,\mathrm{Nm/rad}$ and the damping was chosen such that the link side dynamics is critically damped, i.e., $D_d = 2\sqrt{K_d m} = 40\,\mathrm{Nms/rad}$. At time 0 s, a step of 1 rad is commanded.

The reference controller based on feedback linearization (FBL) does not comply with the control input limitations. For this controller, the gains K_τ and D_τ were chosen as $666.7\,\mathrm{rad}^{-1}\mathrm{s}^{-2}$ and $2.7\,\mathrm{rad}^{-1}\mathrm{s}^{-1}$, respectively. Both MPC controllers were parameterized equally with $Q_\tau = 500\,\mathrm{N}^{-2}\mathrm{m}^{-2}$, $Q_{\dot{\tau}} = 0\,\mathrm{s}^2\mathrm{N}^{-2}\mathrm{m}^{-2}$, and $R = 1 \times 10^{-3}\,\mathrm{N}^{-2}\mathrm{m}^{-2}$. Initially the motor torque of the nominal controller is $1.333 \times 10^5\,\mathrm{Nm}$ due to the step input of the set point and rapidly decreases in the transition phase to $-3.915 \times 10^4\,\mathrm{Nm}$ before it reaches a second peak of 391.5 Nm. For sake of a uniform presentation, the initial phase of the motor torque of the nominal controller is not entirely displayed in Fig. 2. In order to comply with the motor torque limitations, the FBL based control (4) is saturated. This modification severely affects the control action, see Fig. 2. The stability of the overall system can not be guaranteed any more, compare Fig. 3. In the case of MCR and MNR, the control input limitations are included in the control design and the step response yields a stable behavior of the closed-loop system even in this extreme case with a very large step input of the set point.

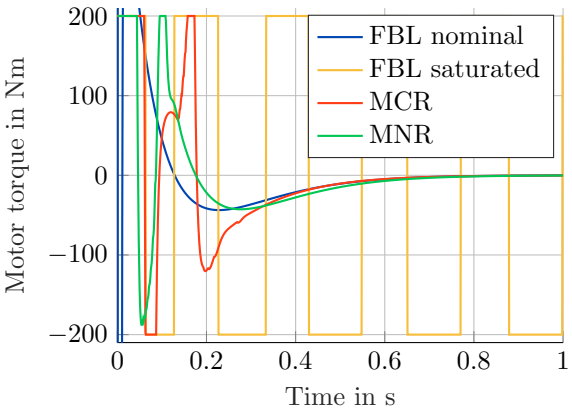

Fig. 2. Motor torque of the simulated step response using compliance control.

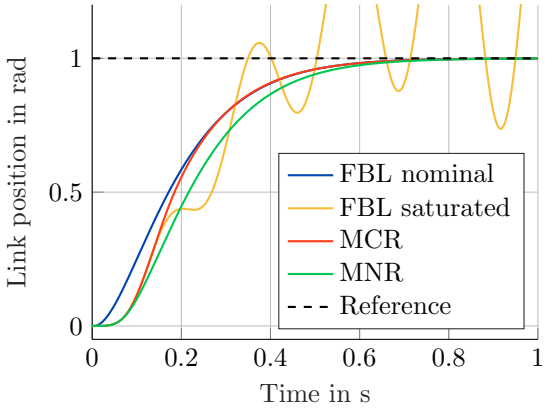

Fig. 3. Link position of the simulated step response using compliance control.

The effect of the different reference designs can be observed in the transient behavior. In the beginning, both controllers apply the maximum motor torque, see Fig. 2. However, MNR reduces the motor torque earlier. This yields a link response which is comparable to the nominal behavior but shifted in time. On the other hand, for MCR the link reaches a higher velocity as in the nominal case. After 0.2 s, the link position of MCR and the nominal controller are almost identical. With regard to the torque error depicted in Fig. 4, MCR produces a significant overshoot of $-92.8\,\mathrm{Nm}$, while for MNR the torque error shows very fast convergence without overshoot.

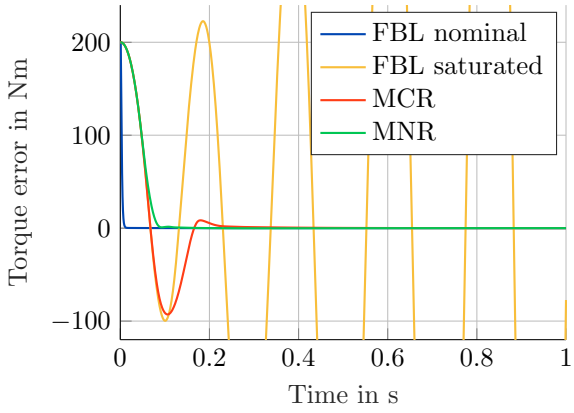

Fig. 4. Torque error of the simulated step response using compliance control.

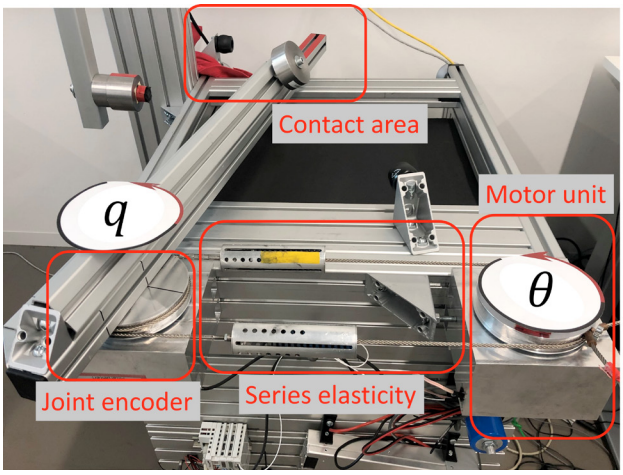

Fig. 5. Setup of the elastic joint testbed.

Motor Inertia B	$0.6\,\mathrm{kgm}^2$
Maximal Motor Torque $\tau_{m,\max}$	$100\,\mathrm{Nm}$
Spring Stiffness K	$374\,\mathrm{Nm/rad}$
Link Inertia M	$1\,\mathrm{kgm}^2$
Controller sample rate	$3\,\mathrm{kHz}$

Table 1. Testbed parameters

5. EXPERIMENTAL VALIDATION

5.1 Experimental Setup and Controller Parameters

The controllers discussed in this paper were evaluated experimentally with a single elastic joint testbed consisting of an off-the-shelf LWR III joint unit (see e.g. Albu-Schäffer et al. (2007)) and a rigid link, which are interconnected by a spring using a steel cable (see Fig. 5). An optical Heidenhain rotary encoder (ECN1023) with 23 bit resolution was used to measure the link side position. The joint torque is obtained by the spring deflection, which is given by the difference between link side and motor position measurements. All relevant parameters of the testbed can be found in Table 1.

To compare the performance of the torque MPC strategy a saturated feedback linearizing control law (4) as in Section 4 was implemented. In the constraint free case, the control parameters of the model predictive controller determine the implemented feedback and feedforward terms. In this case the control law takes the explicit form

$$u_k = -\,[1\ 0\ \dots\ 0]\,\frac{1}{2}\boldsymbol{H}^{-1}\boldsymbol{G} \tag{22}$$

$$= -\,[1\ 0\ \dots\ 0]\,\boldsymbol{H}^{-1}\boldsymbol{P}^T\boldsymbol{F}_u^T\bar{\boldsymbol{Q}}(\boldsymbol{F}_x\boldsymbol{x}_k - \boldsymbol{R}). \tag{23}$$

Thus, the equivalent state feedback gains are obtained by the expression $[1\ 0\ \dots\ 0]\,\boldsymbol{H}^{-1}\boldsymbol{P}^T\boldsymbol{F}_u^T\bar{\boldsymbol{Q}}\boldsymbol{F}_x$. These gains can be used to compare different controller implementations with different weighting parameters. See Table 2 for a complete list of all control parameters.

Torque proportional weight Q_τ	$250\,\mathrm{N}^{-2}\mathrm{m}^{-2}$
Torque derivative proportional weight $Q_{\dot\tau}$	$0.1\,\mathrm{s}^2\mathrm{N}^{-2}\mathrm{m}^{-2}$
Input weight R	$1\times10^{-3}\,\mathrm{N}^{-2}\mathrm{m}^{-2}$
Torque gain K_τ	$3429.8\,\mathrm{rad}^{-1}\mathrm{s}^{-2}$
Torque Derivative gain D_τ	$118.2\,\mathrm{rad}^{-1}\mathrm{s}^{-1}$
Prediction sample time T	$1\times10^{-2}\,\mathrm{s}$
Control Horizon M	10
Prediction Horizon N	10

Table 2. Control parameters of the experimental validation.

5.2 Compliance Control

To validate the control performance a step response of the joint compliance controller (21) is used. At time 0 s, a step of 0.25 rad is commanded for the reference q_d. In the control design, the stiffness of the compliance controller was selected to be $K_d = 100\,\mathrm{Nm/rad}$ and the damping was chosen such that the link side dynamics is critically damped, i.e., $D_d = 2\sqrt{K_d M} = 20\,\mathrm{Nms/rad}$.

Regarding the step response, the MNR performs very similar as the saturated FBL. For both cases, the link converges in the desired critically damped behavior without any overshoot, see Fig. 6. In contrast, the MCR yields a faster response of the link with an overshoot and a transient oscillation. Similarly, the joint torque and its reference for MNR and FBL are almost identical, while MCR has a smaller maximal error but a significant overshoot as depicted in Fig. 7. Figure 8 shows the motor torques. In the initial phase, all controllers max out the full motor torque capabilities. As before, MNR reduces the motor torque earlier than MCR. The saturated FBL based control has a similar temporal course as MNR, however, is considerably more noisy. This is due to the fact, that the feedback law requires higher order time derivatives of $\boldsymbol{\tau}_d$ which are obtained by numerical differentiation. In particular, the feedforward term of $\boldsymbol{B}\boldsymbol{K}^{-1}\ddot{\boldsymbol{\tau}}_d$ generates a disturbing audible noise. The motor torques of the MPC based controllers are less prone to noise amplification. The MNR version still shows a little bit of noise due to the dependency of $\dot{\boldsymbol{\tau}}_d$, while the MCR version shows the most smooth motor torque.

5.3 Contact Experiment

In a second experiment, the link is in contact with a mechanical end stop. A smooth torque reference is commanded and at the end a discontinuous step to zero is performed. See Fig. 9 for a plot of the commanded torque reference and Fig. 10 for the resulting motor torques. The

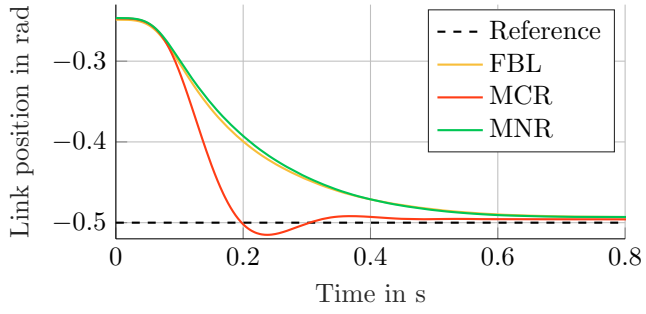

Fig. 6. Joint position of the step response using compliance control.

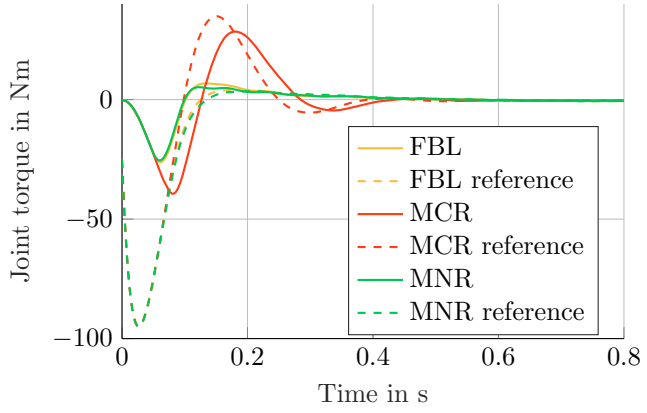

Fig. 7. Joint torques of the step response using compliance control.

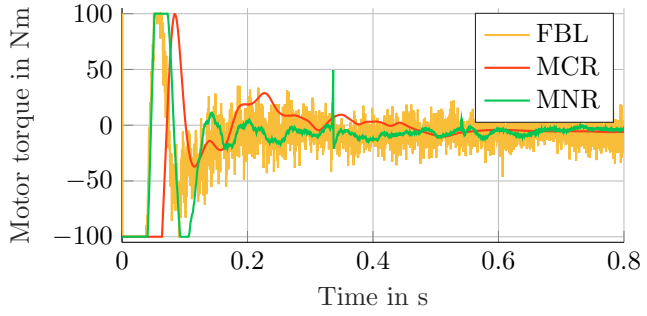

Fig. 8. Motor torques of the step response using compliance control.

experiment is performed for all three controller implementations.

In the initial rising phase, for all controllers the actual torque is below the desired one with FBL achieving the smallest tracking error. When the joint torque reaches approximately 55 Nm the motor torques saturate at 100 Nm and the reference torque can no longer be followed; see also Fig. 10. Crucially, as soon as the joint torque reference becomes feasible again, successful joint torque tracking is reestablished. It is worth pointing out that—immediately after the saturation phase—the convergence rate differs between the different control approaches: 1) FBL shows the highest convergence rate and lowest tracking error, 2) MCR slightly overshoots the reference signal, 3) MNR shows the largest tracking error. The observed deviation for MNR can be explained as follows. Due to reference design for MNR, the computed joint torque reference decreases over time. Thus, MNR applies less motor torque than required to follow the desired signal. This can be clearly seen in Fig. 10. The step response behavior of all three controllers is similar; see Fig. 9 and Fig. 10 from 2 s on wards. In contrast to the free motion experiment, the FBL approach shows significant less motor torque noise. The reason for this is that the joint torque reference terms $(\boldsymbol{\tau}_d, \dot{\boldsymbol{\tau}}_d, \ddot{\boldsymbol{\tau}}_d)$ do not contain (noisy) feedback signals but are given as (noise-free) analytical expressions.

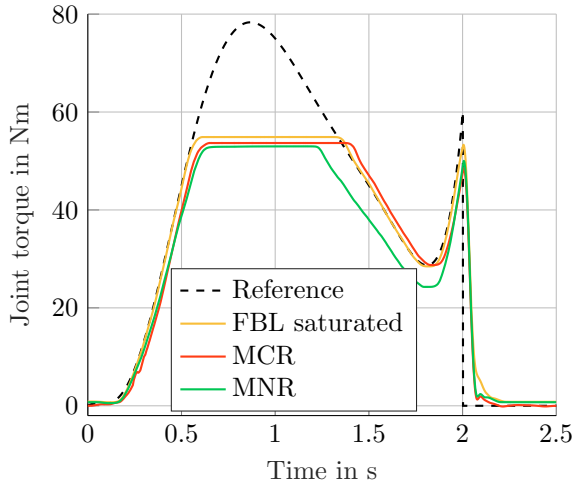

Fig. 9. Joint torques in the contact experiment.

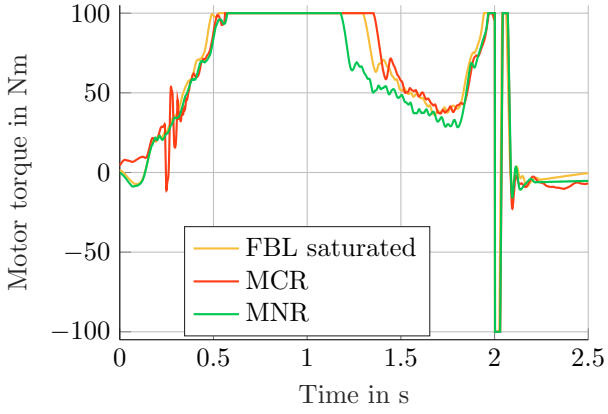

Fig. 10. Motor torque in the contact experiment.

In conclusion, this experiment suggests that all three controllers show robust performance during interaction. In the contact case, however, FBL and MCR achieve a significantly better tracking performance than MNR.

6. SUMMARY AND CONCLUSIONS

In this paper we report experimental results for implementing a low-level joint torque controller via a model predictive control approach, which allows to incorporate constraints on the motor torque into the controller design. The design is motivated by the practically relevant case, in which a high-level (whole-body) controller numerically generates a desired torque for each joint and no differentiable expression of the reference torque is available from analytic computation. In particular we analyzed the use of different reference models in the MPC formulation, namely a constant reference and a reference that follows

the natural open loop dynamics of the elastic joint torque dynamics. From the simulations and experimental results we find that the two approaches considerably differ in the transient behavior. This suggests that a tuning of the QP parameters should not be done independently of the reference model. The presented results focus on a joint torque controller that receives its set points from an outer whole-body or impedance controller. The experimental results furthermore revealed that the MNR version is well suited for realizing a desired torque reference from a high-level controller during free-motion, but its performance for torque tracking of constrained elastic joints was not satisfactory. A more detailed analysis of the MNR controller in contact tasks requires further investigations and is part of our future work.

ACKNOWLEDGEMENTS

The authors would like to thank David Wandinger and Florian Loeffl for their support of the experiments with the elastic actuator testbed.

REFERENCES

Albu-Schäffer, A., Haddadin, S., Ott, C., Stemmer, A., Wimböck, T., and Hirzinger, G. (2007). The dlr lightweight robot – design and control concepts for robots in human environments. *Industrial Robot*, 34, 376–385.

De Luca, A. (1988). Dynamic control of robots with joint elasticity. In *IEEE International Conference on Robotics and Automation*, 152–158 vol.1.

De Luca, A. and Flacco, F. (2010). Dynamic gravity cancellation in robots with flexible transmissions. In *IEEE Conference on Decision and Control (CDC)*, 288–295.

De Luca, A. and Flacco, F. (2011). A pd-type regulator with exact gravity cancellation for robots with flexible joints. In *IEEE international conference on robotics and automation*, 317–323.

Ghahramani, N.O. and Towhidkhah, F. (2009). Constrained incremental predictive controller design for a flexible joint robot. *ISA Transactions*, 48(3), 321–326.

Goodwin, G.C., Carrasco, D.S., Mayne, D.Q., Salgado, M.E., and Serón, M.M. (2011). Preview and feedforward in model predictive control: Conceptual and design issues. *IFAC Proceedings Volumes*, 44(1), 5555–5560. IFAC World Congress.

Henze, B., Roa, M.A., and Ott, C. (2016). Passivity-based whole-body balancing for torque-controlled humanoid robots in multi-contact scenarios. *The International Journal of Robotics Research*, 35(12), 1522–1543.

Keppler, M., Lakatos, D., Ott, C., and Albu-Schäffer, A. (2018). Elastic structure preserving (esp) control for compliantly actuated robots. *IEEE Transactions on Robotics*, 34(2), 317–335.

Keppler, M., Ott, C., and Albu-Schäffer, A. (2022). From underactuation to quasi-full actuation: Aiming at a unifying control framework for articulated soft robots. *International Journal of Robust and Nonlinear Control*.

Kim, M.J., Beck, F., Ott, C., and Albu-Schäffer, A. (2019). Model-free friction observers for flexible joint robots with torque measurements. *IEEE Transactions on Robotics*, 35(6), 1508–1515.

Kuntze, H.b., Jacubasch, A., Richalet, J., and Arber, C. (1986). On the predictive functional control of an elastic industrial robot. In *IEEE Conference on Decision and Control*, 1877–1881.

Liu, B., Ge, W., Zhao, D., Zou, Z., and Li, B. (2020). Mechanical design and energy storage efficiency research of a variable stiffness elastic actuator. *International Journal of Advanced Robotic Systems*, 17(5).

Meduri, A., Shah, P., Viereck, J., Khadiv, M., Havoutis, I., and Righetti, L. (2022). Biconmp: A nonlinear model predictive control framework for whole body motion planning. doi:10.48550/ARXIV.2201.07601. URL `https://arxiv.org/abs/2201.07601`.

Ott, C., Albu-Schäffer, A., Kugi, A., and Hirzinger, G. (2003). Decoupling based cartesian impedance control of flexible joint robots. In *IEEE International Conference on Robotics and Automation*, volume 3, 3101–3107.

Ott, C., Albu-Schäffer, A., Kugi, A., and Hirzinger, G. (2008). On the passivity-based impedance control of flexible joint robots. *IEEE Transactions on Robotics*, 24(2), 416–429.

Palli, G., Melchiorri, C., and De Luca, A. (2008). On the feedback linearization of robots with variable joint stiffness. In *IEEE International Conference on Robotics and Automation*, 1753–1759.

Qin, S. and Badgwell, T.A. (2003). A survey of industrial model predictive control technology. *Control Engineering Practice*, 11(7), 733–764.

Ramuzat, N., Stasse, O., and Boria, S. (2022). Benchmarking whole-body controllers on the talos humanoid robot. *Frontiers in Robotics and AI*, 9.

Sentis, L., Park, J., and Khatib, O. (2010). Compliant control of multicontact and center-of-mass behaviors in humanoid robots. *IEEE Transactions on Robotics*, 26(3), 483–501.

Siciliano, B. and Book, W.J. (1988). A singular perturbation approach to control of lightweight flexible manipulators. *The International Journal of Robotics Research*, 7(4), 79–90.

Spong, M.W. (1987). Modeling and control of elastic joint robots. *Journal of Dynamic Systems, Measurement, and Control*.

Tomei, P. (1991). A simple pd controller for robots with elastic joints. *IEEE Transactions on automatic control*, 36(10), 1208–1213.

Vanderborght, B., Albu-Schäffer, A., Bicchi, A., Burdet, E., Caldwell, D., Carloni, R., Catalano, M., Eiberger, O., Friedl, W., Ganesh, G., Garabini, M., Grebenstein, M., Grioli, G., Haddadin, S., Hoppner, H., Jafari, A., Laffranchi, M., Lefeber, D., Petit, F., Stramigioli, S., Tsagarakis, N., Van Damme, M., Van Ham, R., Visser, L., and Wolf, S. (2013). Variable impedance actuators: A review. *Robotics and Autonomous Systems*, 61(12), 1601–1614.